Steering Law of Control Moment Gyroscopes for Agile Attitude Maneuvers

Takuya Kanzawa,[1] Misuzu Haruki,[2] and Koji Yamanaka[3]
Japan Aerospace Exploration Agency, Tsukuba city, Ibaraki, 305-8505

I. Introduction

Although control moment gyroscopes (CMGs) can produce large torques as compared with the torques produced by reaction wheels (RWs) or momentum wheels (MWs), both practical and theoretical issues remain, such as the singularity problem [1, 2]. Some existing CMG steering methods for attitude maneuvers involve initial gimbal reorientation before slewing and settling. Reorientation is performed to move gimbals to desirable initial angles and to reduce the occurrence of singularities. While the time required to complete gimbal reorientation is shorter than that to complete slewing, the additive gimbal reorientation time would be impossible to ignore if the maneuvers were repeated and would hinder multitarget observations. Thus, it is useful to develop a suitable control/steering law to reduce or eliminate gimbal reorientation time. This study aims to identify, support, and defend a steering law capable of mitigating gimbal reorientation time, which will assist the achievement of agile, large-angle, and rest-to-rest multitarget maneuvers.

In the literature [3, 4], it is assumed that gimbals are positioned at desirable initial angles using solo null motion, namely, a state where gimbals produce no net torque on the spacecraft. Vadali et al. [3] demonstrated the existence of "preferred sets of initial gimbal angles" that avoid singularities, accomplishing singularity-free steering by using a simple pseudo inverse law with initial null motion to position gimbals at their preferred angles. However, pre-slewing gimbal reorientation increases the total maneuver time. One solution to reduce total maneuver time would be to use null motion during each slewing. Schaub et al. [5] proposed a null motion steering law that uses a variable speed CMG (VSCMG). Null motion is continuously used to steer the gimbals toward a less singular configuration, in combination with the steering law that provides the required attitude control torque. Based on the gradient method, the null motion is determined to minimize the singularity measure, which represents how close the gimbal

[1] Associate Senior Engineer, Aerospace Research and Development Directorate, Sengen, Tsukuba city, Ibaraki prefecture. kanzawa.takuya@jaxa.jp
[2] Engineer, Aerospace Research and Development Directorate, Sengen, Tsukuba city, Ibaraki prefecture.
[3] Director of Research Unit I, Research and Development Directorate, Sengen, Tsukuba city, Ibaraki prefecture.

configuration is to singularity, e.g., a condition number of a Jacobian matrix. This approach has merited further investigation into the modification of the singularity measure [6, 7], and into the application of an integrated power and attitude control system (IPACS) [8].

In other works [9 - 11], an optimization technique has been used to determine a gimbal steering profile in advance. The gimbals were steered using a performance index optimization that included the singularity measure, gimbal rate, and attitude tracking errors [10]. However, if optimization parameters are selected to steer the gimbals away from any singularity, the optimization results may constrain the available gimbal steering region, whereupon the resulting gimbal profile may not be applicable to agile and large-angle attitude maneuvers. Conversely, the steering laws aimed at traversing singularities at the expense of torque errors, using the so-called singularity-robust inverse [12 - 16], do not constrain the gimbal steering region. However, a significant issue is that the final gimbal angles, at the completion of each maneuver, may not always match the initial ones. In other words, the gimbals may not always return to their initial angles if the CMGs are steered to compensate for attitude errors by feedback control [9, 10] or to traverse singularities [11, 17, 18]. This issue is referred to as “repeatability” [9, 10, 18]. If the maneuver is repeated several times, the gimbal angles might eventually reach undesirable states, including singularities [17]. Therefore, combining the null motion with a singularity-robust steering law might be effective in securing the end-state gimbal angles.

In this Note, to reduce total maneuver time, a steering law that not only provides the required attitude control torque but also controls the gimbals to the final target gimbal angles, is proposed for conventional CMG (not VSCMG). Until each maneuver is complete, the gimbals are steered to their final target gimbal angles, which are identical to the initial gimbal angles for the subsequent maneuver, thereby eliminating the need for gimbal reorientation between maneuvers. The steering law that do not include gimbal reorientation will enable a spacecraft to continuously perform agile multitarget maneuvers. However, in other works, the behavior of gimbals has not been investigated from the perspective of repeatability. In Sec. II. A, this Note presents a combined torqued- and null-motion steering law that is based on a singularity-robust inverse steering law, as well as a metric to evaluate the contribution of null motion with respect to the total gimbal rate. In Sec. II.B, sets of final target gimbal angles are determined with the condition of rest-to-rest maneuvers and the stability of gimbal angle control is analyzed using a Lyapunov function. A quadratic form, in accordance with the magnitude of null motion, is proposed to evaluate whether null motion can effectively control the gimbal angle. This analysis clearly explains the mechanisms of

gimbal angle convergence and shows that gimbals may not converge to their final target angles when the quadratic form becomes too small. In Sec. III, to resolve the aforementioned repeatability issue, the steering law is modified by including a weighting matrix that depends on the prescribed attitude control torque profile. Finally, in Sec. IV, a total of 66 numerical simulations for agile multitarget maneuvers are conducted to verify the overall effectiveness and performance of the proposed steering law. Some performance metrics related to singularity identify sets of desirable final gimbal angles that improve the performances resulting from conventional steering laws [3, 14].

II. Combined Steering Law and Its Properties

A. Steering Law Overview

As proposed in Sec. I, the null motion $\dot{\boldsymbol{\delta}}_{\mathrm{NV}}$ to control the gimbals to the final target angles is superimposed onto the torqued motion $\dot{\boldsymbol{\delta}}_{\mathrm{TV}}$ to provide attitude control torque. The total gimbal rate command $\dot{\boldsymbol{\delta}}_{\mathrm{V}}$ is expressed using the weighting matrix $\mathbf{V} \in \mathrm{R}^{3\times 3}$ proposed in the singularity-robust inverse [12 - 16] as follows:

$$\dot{\boldsymbol{\delta}}_{\mathrm{V}} = \frac{1}{\mathrm{h}_{\mathrm{R}}} \mathbf{A}^{\mathrm{T}} \left(\mathbf{A}\mathbf{A}^{\mathrm{T}} + \mathbf{V} \right)^{-1} \cdot \mathbf{u} + \mathrm{K}_{\mathrm{N}} \, \mathbf{S}_{\mathrm{V}} \left(\boldsymbol{\delta}_{\mathrm{F}} - \boldsymbol{\delta} \right) \equiv \dot{\boldsymbol{\delta}}_{\mathrm{TV}} + \dot{\boldsymbol{\delta}}_{\mathrm{NV}} \tag{1}$$

where scalar K_{N} (> 0) is the null motion gain that represents the amount of null motion. We assume that the final target gimbal angles $\boldsymbol{\delta}_{\mathrm{F}} \in \mathrm{R}^{4\times 1}$ are determined as constant values in advance, which will be discussed in Sec. II.B. The required attitude control torque command $\mathbf{u} \in \mathrm{R}^{3\times 1}$ is expressed as follows:

$$\mathbf{u} \equiv \dot{\mathbf{H}} = -\left(\mathbf{T}_{\mathrm{CNT}}^{\mathrm{ff}} + \mathbf{T}_{\mathrm{CNT}}^{\mathrm{fb}} \right) - \tilde{\boldsymbol{\omega}} \mathbf{H} = \mathrm{h}_{\mathrm{R}} \mathbf{A} \dot{\boldsymbol{\delta}} \tag{2}$$

The feedforward control torque $\mathbf{T}_{\mathrm{CNT}}^{\mathrm{ff}} \in \mathrm{R}^{3\times 1}$ is generated as a prescribed bang-off-bang torque profile [19, 20], i.e., acceleration and deceleration torque periods are separated by a coasting period. The feedback control torque $\mathbf{T}_{\mathrm{CNT}}^{\mathrm{fb}} \in \mathrm{R}^{3\times 1}$ compensates for the tracking errors with respect to the attitude rate profile $\boldsymbol{\omega}_{\mathrm{REF}} \in \mathrm{R}^{3\times 1}$ and angle profile $\boldsymbol{\Theta}_{\mathrm{REF}} \in \mathrm{R}^{3\times 1}$.

$$\mathbf{T}_{\mathrm{CNT}}^{\mathrm{fb}} = \mathbf{K}_{\mathrm{d}} \left(\boldsymbol{\omega}_{\mathrm{REF}} - \boldsymbol{\omega} \right) + \mathbf{K}_{\mathrm{p}} \left(\boldsymbol{\Theta}_{\mathrm{REF}} - \boldsymbol{\Theta} \right) \tag{3}$$

where $\mathbf{K}_{\mathrm{d}} \in \mathrm{R}^{3\times 3}$ and $\mathbf{K}_{\mathrm{p}} \in \mathrm{R}^{3\times 3}$ denote diagonal constant derivative and proportional gain matrices, respectively.

The following two matrices, including the weighting matrix $\mathbf{V}$, are defined and named as "generalized projection matrices" in this Note.

$$\mathbf{P}_V \equiv \mathbf{A}^T\left(\mathbf{A}\mathbf{A}^T + \mathbf{V}\right)^{-1}\mathbf{A}, \quad \mathbf{S}_V \equiv \mathbf{U}_{44} - \mathbf{P}_V \tag{4}$$

Because the weighting matrix $\mathbf{V}$ is selected as symmetric [12 - 16], these matrices remain symmetric ($\mathbf{P}_V{}^T = \mathbf{P}_V$, $\mathbf{S}_V{}^T = \mathbf{S}_V$) even in the vicinity of a singularity but not idempotent ($\mathbf{P}_V{}^2 \neq \mathbf{P}_V$, $\mathbf{S}_V{}^2 \neq \mathbf{S}_V$). On the contrary, the matrices $\mathbf{P} \equiv \mathbf{A}^+\mathbf{A} = \mathbf{A}^T\left(\mathbf{A}\mathbf{A}^T\right)^{-1}\mathbf{A} \in \mathrm{R}^{4\times 4}$ and $\mathbf{S} \equiv \mathbf{U}_{44} - \mathbf{P} \in \mathrm{R}^{4\times 4}$, known as orthogonal projection matrices, have two basic properties: they are idempotent ($\mathbf{P}^2 = \mathbf{P}$, $\mathbf{S}^2 = \mathbf{S}$) and symmetric ($\mathbf{P}^T = \mathbf{P}$, $\mathbf{S}^T = \mathbf{S}$) [21]. Using the symmetric matrix $\mathbf{S}_V$, the stability of the gimbal angle control can be discussed on the basis of the quadratic form defined in Sec. II.B. As the gimbals approach a singularity (CMG gain $\mathrm{m} = \sqrt{\det\left(\mathbf{A}\mathbf{A}^T\right)} \approx 0$), the weighting matrix $\mathbf{V}$ becomes large and guarantees the non-singularity of the matrices $\mathbf{A}^T\left(\mathbf{A}\mathbf{A}^T + \mathbf{V}\right)^{-1}$ and $\mathbf{S}_V$ in Eq. (1). Consequently, the steering law enables both torqued and null motions, even when the CMG system encounters a singularity.

In the following analysis, it is shown that the null motion contribution, with respect to the total gimbal rate, changes according to the distance from singularity. Let γ_V be the angle between the torqued motion $\dot{\boldsymbol{\delta}}_{TV}$ and the total gimbal rate $\dot{\boldsymbol{\delta}}_V$. When the gimbal configuration is near to singularity, γ_V is defined using $\dot{\boldsymbol{\delta}}_{TV}$ and $\dot{\boldsymbol{\delta}}_V$, as follows:

$$\cos\gamma_V = \frac{\dot{\boldsymbol{\delta}}_{TV}{}^T\dot{\boldsymbol{\delta}}_V}{\left|\dot{\boldsymbol{\delta}}_{TV}\right|\left|\dot{\boldsymbol{\delta}}_V\right|} \tag{5}$$

When the gimbal configuration is far from singularity, the weighting matrix $\mathbf{V}$ in Eq. (1) can be neglected. Then, the torqued- and null-motion using the pseudo inverse matrix $\mathbf{A}^+ = \mathbf{A}^T\left(\mathbf{A}\mathbf{A}^T\right)^{-1}$ and orthogonal projection matrix $\mathbf{S}$ are defined as $\dot{\boldsymbol{\delta}}_T$ and $\dot{\boldsymbol{\delta}}_N$, respectively. The null motion is perpendicular to the torqued motion when far from singularity ($\dot{\boldsymbol{\delta}}_T^T\dot{\boldsymbol{\delta}}_N = 0$), although they are not perpendicular when near to singularity ($\dot{\boldsymbol{\delta}}_{TV}^T\dot{\boldsymbol{\delta}}_{NV} \neq 0$). Accordingly, the two-norm of the total gimbal rate $\dot{\boldsymbol{\delta}}$ satisfies the following condition:

$$\left|\dot{\boldsymbol{\delta}}\right|^2 = \left|\dot{\boldsymbol{\delta}}_T + \dot{\boldsymbol{\delta}}_N\right|^2 = \left|\dot{\boldsymbol{\delta}}_T\right|^2 + \left|\dot{\boldsymbol{\delta}}_N\right|^2 \geq \left|\dot{\boldsymbol{\delta}}_T\right|^2 \tag{6}$$

Taking into account the properties of the orthogonal projection matrices $\mathbf{P}$ and $\mathbf{S}$, the relationships $\dot{\boldsymbol{\delta}}_T = \mathbf{P}\dot{\boldsymbol{\delta}}$ and $\dot{\boldsymbol{\delta}}_N = \mathbf{S}\dot{\boldsymbol{\delta}}$ can be simply proved [21]. Consequently, the two-norm of torqued motion $\dot{\boldsymbol{\delta}}_T$ and null motion $\dot{\boldsymbol{\delta}}_N$, represented in Eq. (6), can be written as follows:

$$\left|\dot{\boldsymbol{\delta}}_T\right|^2 = \dot{\boldsymbol{\delta}}_T^T\dot{\boldsymbol{\delta}}_T = \dot{\boldsymbol{\delta}}^T\mathbf{P}^T\mathbf{P}\dot{\boldsymbol{\delta}} = \dot{\boldsymbol{\delta}}^T\mathbf{P}^2\dot{\boldsymbol{\delta}} = \dot{\boldsymbol{\delta}}^T\mathbf{P}\dot{\boldsymbol{\delta}} \tag{7}$$

$$\left|\dot{\boldsymbol{\delta}}_N\right|^2 = \dot{\boldsymbol{\delta}}_N^T\dot{\boldsymbol{\delta}}_N = \dot{\boldsymbol{\delta}}^T\mathbf{S}^T\mathbf{S}\dot{\boldsymbol{\delta}} = \dot{\boldsymbol{\delta}}^T\mathbf{S}^2\dot{\boldsymbol{\delta}} = \dot{\boldsymbol{\delta}}^T\mathbf{S}\dot{\boldsymbol{\delta}} \tag{8}$$

Eq. (5) can be rewritten using the relations $\dot{\boldsymbol{\delta}}_T{}^T\dot{\boldsymbol{\delta}} = \dot{\boldsymbol{\delta}}_T{}^T\dot{\boldsymbol{\delta}}_T = \left|\dot{\boldsymbol{\delta}}_T\right|^2$ and $\mathbf{P}+\mathbf{S} = \mathbf{U}_{44}$, as well as Eqs. (7) and (8).

$$\cos\gamma_V = \frac{\dot{\boldsymbol{\delta}}_T{}^T\dot{\boldsymbol{\delta}}}{\left|\dot{\boldsymbol{\delta}}_T\right|\left|\dot{\boldsymbol{\delta}}\right|} = \frac{\left|\dot{\boldsymbol{\delta}}_T\right|}{\left|\dot{\boldsymbol{\delta}}\right|} = \sqrt{\frac{\dot{\boldsymbol{\delta}}^T\mathbf{P}\dot{\boldsymbol{\delta}}}{\dot{\boldsymbol{\delta}}^T\dot{\boldsymbol{\delta}}}} = \sqrt{1-\frac{\dot{\boldsymbol{\delta}}^T\mathbf{S}\dot{\boldsymbol{\delta}}}{\dot{\boldsymbol{\delta}}^T\dot{\boldsymbol{\delta}}}} \tag{9}$$

Eq. (9) indicates that the angle γ_V can be taken at the range $0 \le \cos\gamma_V \le 1$. When far from singularity, the null motion need not steer the gimbals to the final target angles $\boldsymbol{\delta}_F$, because the gimbals return there naturally, which indicates that the null motion is relatively small with respect to the total gimbal rate ($\cos\gamma_V \approx 1$). Conversely, Eq. (5) indicates that the angle γ_V can be taken at the range $-1 \le \cos\gamma_V \le 1$. As the gimbals approach a singularity, the null motion is increased to steer the gimbals to the final angles $\boldsymbol{\delta}_F$, which indicates that the null motion becomes relatively large with respect to the total gimbal rate ($\cos\gamma_V \approx 0$). When near to singularity, the null motion is further increased ($\cos\gamma_V \approx -1$).

B. Stability of Gimbal Angle Control

As proposed in Sec. I, the gimbals are steered to the final target gimbal angles $\boldsymbol{\delta}_F^i$ by the end of the i-th maneuver. In the subsequent (i + 1)th maneuver, the gimbals are steered from the initial angles $\boldsymbol{\delta}_0^{i+1}$ and toward the final angles from the previous i-th maneuver ($\boldsymbol{\delta}_0^{i+1} = \boldsymbol{\delta}_F^i$). Such gimbal angle control will enable the spacecraft to perform continuous multitarget maneuvers without gimbal reorientation delay. A key issue in this approach is how to determine the final gimbal angles. Computing the final angles for general maneuvering scenarios is challenging. Furthermore, null motion is only available for a limited set of gimbal angles. For example, reconfiguring a symmetric set of gimbal angles into an asymmetric set without exerting torques on the spacecraft is impossible [5]. In our approach, the final angles are limited to symmetric sets with the condition of rest-to-rest maneuvers, which

means that the total angular momentum produced by the CMG system should be equal to zero at the end of each maneuver. Although some gimbal angle sets satisfying the zero momentum condition exist, here, we consider only one symmetric set: $\boldsymbol{\delta}_F = \begin{bmatrix} d_1 & d_2 & d_1 & d_2 \end{bmatrix}^T$ ($-\pi \le d_1, d_2 \le \pi$ rad). Substituting this set into the zero momentum condition $\mathbf{H} = \mathbf{O}_{31}$, the following two sets are obtained: $\boldsymbol{\delta}_{Fa} = \begin{bmatrix} d & -d & d & -d \end{bmatrix}^T$ rad and $\boldsymbol{\delta}_{Fb} = \begin{bmatrix} d & d-\pi & d & d-\pi \end{bmatrix}^T$ rad.

The stability of gimbal reorientation using solo null motion is analyzed in the literature [3]. In this section, the stability of the gimbal angle control to the aforementioned symmetric sets is analyzed using both torqued and null motions. The Lyapunov function is simply selected as the two-norm of gimbal angle errors $\mathbf{e} = \boldsymbol{\delta}_F - \boldsymbol{\delta}$, as follows:

$$L_V = \frac{1}{2}\mathbf{e}^T\mathbf{e} = \frac{1}{2}(\boldsymbol{\delta}_F - \boldsymbol{\delta})^T(\boldsymbol{\delta}_F - \boldsymbol{\delta}) \tag{10}$$

The time derivative of L_V can be represented by substituting the steering law of Eq. (1):

$$\dot{L}_V = -(\boldsymbol{\delta}_F - \boldsymbol{\delta})^T\dot{\boldsymbol{\delta}}_V = -\mathbf{e}^T\dot{\boldsymbol{\delta}}_{TV} - \mathbf{e}^T\dot{\boldsymbol{\delta}}_{NV} \equiv \eta_{TV} - K_N\eta_{SV} \tag{11}$$

where

$$\eta_{TV} \equiv -\mathbf{e}^T\dot{\boldsymbol{\delta}}_{TV} = -\frac{1}{h_R}\mathbf{e}^T\mathbf{A}^T\left(\mathbf{A}\mathbf{A}^T + \mathbf{V}\right)^{-1}\mathbf{u} \tag{12}$$

$$\eta_{SV} \equiv \mathbf{e}^T\bar{\dot{\boldsymbol{\delta}}}_{NV} = \mathbf{e}^T\mathbf{S}_V\mathbf{e} \tag{13}$$

$\bar{\dot{\boldsymbol{\delta}}}_{NV}$ denotes the unit null motion, where the null motion gain K_N is equal to one. The Lyapunov function L_V at an arbitrary time t in the maneuver duration $t_0 \le t \le t_F$ is again obtained by integrating Eq. (11).

$$L_V(t) = L_V(t_0) + \int_{t_0}^{t}\dot{L}_V(\tau)d\tau \equiv L_{TV}(t) + L_{SV}(t) \tag{14}$$

where

$$L_{TV}(t) \equiv \int_{t_0}^{t}\eta_{TV}d\tau\,, \quad L_{SV}(t) \equiv L_V(t_0) - \int_{t_0}^{t}K_N\eta_{SV}d\tau \tag{15}$$

Note that Eq. (14) shows that the Lyapunov function can be separated into two terms, where the first term L_{TV} depends on the torqued motion $\dot{\boldsymbol{\delta}}_{TV}$ and the second term L_{SV} depends on the null motion $\dot{\boldsymbol{\delta}}_{NV}$. As described below, this allows us to consider the behavior of these terms individually.

The torque command $\mathbf{u}$ of Eq. (2) satisfies the conditions $\mathbf{u}(t_0) = \mathbf{O}_{31}$ and $\mathbf{u}(t_F) = \mathbf{O}_{31}$, because the rest-to-rest maneuvers are dealt with in the present study. The initial condition for Eq. (15) is therefore $L_{TV}(t_0) = 0$, and the final state $L_{TV}(t_F)$ converges to a certain constant value at the end of each maneuver.

The quadratic form η_{SV} of Eq. (13), including the symmetric matrix $\mathbf{S}_V$, plays an important role in evaluating the stability of the gimbal angle control. Excluding the torqued motion $\dot{\boldsymbol{\delta}}_{TV}$ in Eq. (1), the steering law is regarded as a nonlinear dynamical system $\dot{\mathbf{e}} = f(\mathbf{e}) = -K_N \mathbf{S}_V \mathbf{e}$ in terms of gimbal angle error $\mathbf{e}$. Because of the fact that the generalized projection matrix $\mathbf{S}_V$ is a time-varying matrix, which depends on the current gimbal angles $\boldsymbol{\delta}$ and the weighting matrix $\mathbf{V}$, definiteness is examined for two quadratic forms, $\eta_S = \mathbf{e}^T \mathbf{S} \mathbf{e}$ and $\eta_{SV} = \mathbf{e}^T \mathbf{S}_V \mathbf{e}$, for cases that are far-from- and near-to-singularity, respectively. For cases that are far from singularity, the quadratic form is a positive semidefinite ($\eta_S \geq 0$), because the orthogonal projection matrix $\mathbf{S}$ is idempotent and its eigenvalues are either 0 or 1. Moreover, it can easily be shown that the quadratic form η_S is transformed into the two-norm of the unit null motion using the properties described in Sec. II.A.

$$\eta_S = \mathbf{e}^T \mathbf{S} \mathbf{e} = \mathbf{e}^T \mathbf{S}^T \mathbf{S} \mathbf{e} = \bar{\dot{\boldsymbol{\delta}}}_N{}^T \bar{\dot{\boldsymbol{\delta}}}_N = \left| \bar{\dot{\boldsymbol{\delta}}}_N \right|^2 \geq 0 \tag{16}$$

In general, for cases that are near singularity, the eigenvalues of the generalized projection matrix $\mathbf{S}_V$ are only real numbers, because $\mathbf{S}_V$ is only symmetric. Accordingly, the following Rayleigh–Ritz inequality [22] is employed to examine the positive semidefinite of $\eta_{SV} = \mathbf{e}^T \mathbf{S}_V \mathbf{e}$:

$$\lambda_{min} \mathbf{e}^T \mathbf{e} \leq \mathbf{e}^T \mathbf{S}_V \mathbf{e} \leq \lambda_{max} \mathbf{e}^T \mathbf{e} \tag{17}$$

where λ_{min} and λ_{max} are the smallest and largest eigenvalues of $\mathbf{S}_V$, respectively. It can be verified by numerical simulations that the eigenvalues λ_i (i = 1 to 4) in the singularity are always within the range $0 \leq \lambda_i \leq 1$, indicating that the above inequality should be rewritten as $0 \leq \eta_{SV} \leq \mathbf{e}^T \mathbf{e} = 2L_V$. As shown above, the two quadratic forms are positive semidefinite, both when far-from- and near-to-singularity; therefore, the null motion term L_{SV} of Eq. (15) is guaranteed to be asymptotically stable. In other words, L_{SV} is decreased from its initial value $L_V(t_0) = L_{SV}(t_0) = 1/2\, \mathbf{e}_0^T \mathbf{e}_0$, which is written as follows:

$$L_{SV}(t) = \frac{1}{2}\mathbf{e}_0{}^T\mathbf{e}_0 - \int_{t_0}^{t} K_N \eta_{SV} d\tau \le \frac{1}{2}\mathbf{e}_0{}^T\mathbf{e}_0 \tag{18}$$

As shown later in Sec. V, the quadratic form $\eta_{SV} = \mathbf{e}^T\mathbf{S}_V\mathbf{e}$ is increased unlike the CMG gain, which decreased in the vicinity of a singularity ($m \to 0$). This implies that the null motion term L_{SV} is smaller after traversing singularity. From Eqs. (14) and (18), it can be concluded that if L_{SV} declines sufficiently to cancel out the torqued motion term L_{TV} by the end of each maneuver, the total Lyapunov function L_V converges to zero, as does the resulting gimbal angle error $\mathbf{e}$.

From Eq. (18), however, it is estimated that the gimbal angles $\boldsymbol{\delta}$ may not converge to the final target angles $\boldsymbol{\delta}_F$, if the quadratic form η_{SV} becomes too small. From linear algebra, $\eta_{SV} = \mathbf{e}^T\mathbf{S}_V\mathbf{e} = \mathbf{e}^T\bar{\dot{\boldsymbol{\delta}}}_{NV} = 0$ if and only if $\bar{\dot{\boldsymbol{\delta}}}_{NV} = \mathbf{O}_{41}$ is satisfied because the generalized projection matrix $\mathbf{S}_V$ is symmetric and positive semidefinite ($\mathbf{S}_V \ge 0$). From this relation, it is apparent that the unit null motion becomes small ($\bar{\dot{\boldsymbol{\delta}}}_{NV} \approx \mathbf{O}_{41}$) when the quadratic form becomes small ($\eta_{SV} \approx 0$). Consequently, the null motion $\dot{\boldsymbol{\delta}}_{NV}$ will be too small to control the gimbals to the final target angles effectively. Whether or not null motion is possible depends on the type of singularity, hyperbolic or elliptic, and a test can be used to identify them [23 - 25]. Null motion is possible near a hyperbolic singularity and is not possible near an elliptic singularity. The convergence mechanism of the gimbal angles, described in this section, is demonstrated by the numerical simulations shown in Sections IV.C and IV.D. Furthermore, the steering law proposed in Sec. II.A will be modified in Sec. III to resolve the aforementioned repeatability issue [9 - 11, 17, 18].

III. Modification of the Steering Law

As pointed out in Sec. II.B, the unit null motion itself ($\bar{\dot{\boldsymbol{\delta}}}_{NV} = \mathbf{S}_V\mathbf{e}$) may become too small for gimbal control, even if the null motion gain K_N is large. A suitable modification for the steering law of Eq. (1) is therefore considered to prevent the unit null motion from becoming too small to be effective. For this purpose, we now reconsider the following two-norm and least-squares minimization problem [14, 15]:

$$\min_{\dot{\boldsymbol{\delta}}_{TVW}} \left(\dot{\boldsymbol{\delta}}_{TVW}^T \mathbf{Q} \dot{\boldsymbol{\delta}}_{TVW} + \bar{\mathbf{u}}_{err}^T \mathbf{R} \bar{\mathbf{u}}_{err} \right) \tag{19}$$

where $\mathbf{Q} \equiv \mathbf{W}^{-1} \in \mathrm{R}^{4\times4}$ and $\mathbf{R} \equiv \mathbf{V}^{-1} \in \mathrm{R}^{3\times3}$ are positive definite symmetric weighting matrices, i.e., $\mathbf{Q} = \mathbf{Q}^{\mathrm{T}} > 0$, $\mathbf{R} = \mathbf{R}^{\mathrm{T}} > 0$, and $\overline{\mathbf{u}}_{\mathrm{err}} = \overline{\mathbf{u}} - \mathbf{A}\dot{\boldsymbol{\delta}}$ represents the unit torque error where the rotor angular momentum h_{R} is equal to one. The solution of Eq. (19) in the case of $\mathbf{W} \neq \mathbf{U}_{44}$ is derived as $\dot{\boldsymbol{\delta}}_{\mathrm{TVW}} = 1/\mathrm{h}_{\mathrm{R}}\, \mathbf{W}\mathbf{A}^{\mathrm{T}}\left(\mathbf{A}\mathbf{W}\mathbf{A}^{\mathrm{T}} + \mathbf{V}\right)^{-1}\mathbf{u}$ [15]. The torqued motion $\dot{\boldsymbol{\delta}}_{\mathrm{TV}}$ in Eq. (1) can be obtained by solving Eq. (19), in the case of $\mathbf{W} = \mathbf{U}_{44}$. Here as well as in Eq. (1), null motion $\dot{\boldsymbol{\delta}}_{\mathrm{NVW}}$, including $\mathbf{W} \neq \mathbf{U}_{44}$, is also defined and the total gimbal rate command $\dot{\boldsymbol{\delta}}_{\mathrm{VW}}$ is written as follows:

$$\dot{\boldsymbol{\delta}}_{\mathrm{VW}} = \frac{1}{\mathrm{h}_{\mathrm{R}}}\mathbf{W}\mathbf{A}^{\mathrm{T}}\left(\mathbf{A}\mathbf{W}\mathbf{A}^{\mathrm{T}} + \mathbf{V}\right)^{-1}\cdot\mathbf{u} + \mathrm{K}_{\mathrm{N}}\,\mathbf{S}_{\mathrm{VW}}\left(\boldsymbol{\delta}_{\mathrm{F}} - \boldsymbol{\delta}\right) \equiv \dot{\boldsymbol{\delta}}_{\mathrm{TVW}} + \dot{\boldsymbol{\delta}}_{\mathrm{NVW}} \tag{20}$$

The generalized projection matrices, including $\mathbf{W} \neq \mathbf{U}_{44}$, are newly defined by

$$\mathbf{P}_{\mathrm{VW}} \equiv \mathbf{W}\mathbf{A}^{\mathrm{T}}\left(\mathbf{A}\mathbf{W}\mathbf{A}^{\mathrm{T}} + \mathbf{V}\right)^{-1}\mathbf{A}, \quad \mathbf{S}_{\mathrm{VW}} \equiv \mathbf{U}_{44} - \mathbf{P}_{\mathrm{VW}} \tag{21}$$

The weighting matrix $\mathbf{W} \neq \mathbf{U}_{44}$ is expected to change for the matrix $\mathbf{S}_{\mathrm{VW}}$ in Eq. (20) and effectively boost the null motion $\dot{\boldsymbol{\delta}}_{\mathrm{NVW}}$. To modify the convergence to the final target gimbal angles $\boldsymbol{\delta}_{\mathrm{F}}$, appropriate weight must be given to the steering law as the gimbals approach their final angles in the final stage of each maneuver. Because the duration of the gimbals' approach to their final angles can be regarded as equivalent to the duration that the CMG system is producing deceleration torque, information on the feedforward torque profile $\mathbf{T}_{\mathrm{CNT}}^{\mathrm{ff}}$ can be provided to the steering law by the control law. Accordingly, the weighting matrix $\mathbf{W}$ during gimbals' approach is given by

$$\mathbf{W} = \lambda_{\mathrm{W}}\mathbf{E}_{\mathrm{W}} = \lambda_{\mathrm{W}}\cdot\mathrm{diag}\left[\varepsilon_{\mathrm{W1}} \quad \varepsilon_{\mathrm{W2}} \quad \varepsilon_{\mathrm{W3}} \quad \varepsilon_{\mathrm{W4}}\right] \tag{22}$$

wherein

$$\lambda_{\mathrm{W}} = \lambda_{\mathrm{W0}}\mathrm{e}^{-\mu_{\mathrm{w}}\tau}, \quad \tau = \left|\mathbf{T}_{\mathrm{CNT}}^{\mathrm{ff}}\right| \Big/ \left|\mathbf{T}_{\mathrm{CNT}}^{\mathrm{ff}}\right|^{\max} \tag{23}$$

where the scalar λ_{W} is a time-varying scaling factor adjusted by the normalized torque profile τ, the range of which is $0 \le \tau \le 1$. The other scalars, i.e., λ_{W0}, μ_{W}, and $\varepsilon_{\mathrm{Wi}}$ (i = 1–4), are constant parameters to be properly selected. Note that new generalized projection matrices of Eq. (21) are neither idempotent nor symmetric, i.e., $\mathbf{P}_{\mathrm{VW}}{}^{2} \neq \mathbf{P}_{\mathrm{VW}}$, $\mathbf{S}_{\mathrm{VW}}{}^{2} \neq \mathbf{S}_{\mathrm{VW}}$, $\mathbf{P}_{\mathrm{VW}}{}^{\mathrm{T}} \neq \mathbf{P}_{\mathrm{VW}}$, and $\mathbf{S}_{\mathrm{VW}}{}^{\mathrm{T}} \neq \mathbf{S}_{\mathrm{VW}}$. Because $\mathbf{S}_{\mathrm{VW}}$ is not a symmetric matrix, the quadratic form $\eta_{\mathrm{SVW}} = \mathbf{e}^{\mathrm{T}}\mathbf{S}_{\mathrm{VW}}\mathbf{e}$ cannot be strictly defined and the stability of the gimbal angle control cannot be

analyzed, as shown in Sec. II.B. Despite this, the convergence of the gimbal angles by the modified steering law that includes $\mathbf{S}_{VW}$ is numerically verified in Sec. IV.D.

IV. Numerical Simulations

A. Simulation Parameters

To verify the effectiveness and performance of the proposed steering law, agile multitarget maneuvers are numerically simulated, the parameters for which are shown in Table 1. It is assumed that a mid-sized Earth-observing spacecraft performs ten large-angle, rest-to-rest, and bang-off-bang maneuvers. In the spacecraft body-fixed coordinate $\{\vec{\mathbf{b}}_B\}$, the maneuver axes are aligned into the roll–pitch ($\vec{\mathbf{b}}_{Bx} - \vec{\mathbf{b}}_{By}$) plane to change the direction of the pointing axis $\vec{\mathbf{b}}_{Bz}$ toward multiple targets on the ground. The feedforward torque profile $\mathbf{T}_{CNT}^{ff}$ has trapezoidal shapes during the acceleration and deceleration periods. In the first maneuver, the spacecraft performs slewing from an initial attitude $[0\ 0\ 0]^T$ deg to a final attitude $[50\ 50\ 0]^T$ deg within 70 s (from t_0=10 s to t_F=80 s) about maneuver axis $1/\sqrt{2} \times [1\ \ 1\ \ 0]^T$, while attitude errors are subsequently settled by feedback control. Similarly, the second maneuver is performed in the opposite direction within 70 s (from t_0=100 s to t_F=170 s). The remaining maneuvers are repeated, as well as the first and second maneuvers. To compensate for the tracking errors with respect to the attitude profiles $\boldsymbol{\omega}_{REF}$ and $\boldsymbol{\Theta}_{REF}$, the derivative and proportional gains in Eq. (3) are determined using the high-bandwidth $f_S = 0.5\text{Hz}$ and the damping ratio $\zeta_S = 1/\sqrt{2}$. The parameters for weighting matrix $\mathbf{V}$ are similar to those used in the GSR steering law [14]. The gimbal rate command is limited within $\dot{\delta}_i^{lmt} = \pm 1.0\text{rad/s}$ (i = 1 –4) for each CMG, because of practical hardware capabilities.

B. Performance of the Steering Law

First, the simulation results from applying the GSR steering law, i.e., null motion gain $K_N = 0$ in Eq. (1), are shown in Figure 1 as Case 1. As illustrated in Figure 1a, the final gimbal angles after each maneuver are not the same as the initial gimbal angles, i.e., the gimbals are not repeatable, as is stated in the literature [18]. This indicates that the GSR, using solo torqued motion, is unable to secure the final gimbal states after traversing singularities. Figure 1b illustrates the gimbal rate command $\dot{\boldsymbol{\delta}}_{TV}$, taking into consideration the gimbal rate limit, and Figure 1c

demonstrates how the CMG system encounters singularities over a series of ten maneuvers. After the CMG system encounters singularity ($m \approx 0$) at approximately 750 s., it loses the capability to provide the required torque and eventually retains the singularity until the end of the 10th maneuver.

Next, a total of 66 simulation runs are conducted for various sets of final gimbal angles $\boldsymbol{\delta}_F$ to verify the overall performance of the steering law (Eq. (1)). Figure 2 summarizes the results for the first set of simulations, which are named as Case 2 in accordance with $\boldsymbol{\delta}_{Fa} = [d \; -d \; d \; -d]^T$ rad. The 37 cases are investigated using various gimbal angles d, as plotted in circles as shown in Figure 2a. Similarly, Figure 3 summarizes the results for the second set of 29 cases, which are named as Case 3 in accordance with $\boldsymbol{\delta}_{Fb} = [d \; d-\pi \; d \; d-\pi]^T$ rad. To ensure a fair comparison, the three performance metrics related to the singularity are defined as follows: 1) the mean value of the CMG gain $m = \sqrt{\det\left(\mathbf{A}\mathbf{A}^T\right)}$ (bars in Figures 2a and 3a), 2) the number of times traversing the singularities s_{m0} (bars in Figures 2b and 3b), and 3) the total duration in singularities t_{m0} (bars in Figures 2c and 3c). Here, the metric s_{m0} represents the number of times the CMG gain becomes smaller than threshold $m_{thr} = 0.2$, and the metric t_{m0} represents duration of the singularities, which are defined as $m < m_{thr}$. The simulations terminate when t_{m0} exceeds 10% of the total simulation time (900 s). These metrics are compared with those of the aforementioned GSR (Case 1), i.e., the results of Figure 1 are plotted as a dotted line in both Figures 2 and 3.

As for Case 2 (Figure 2), the gimbals converge to the final target gimbal angles $\boldsymbol{\delta}_{Fa}$ in case of d = −15, −10, 0, 10, 15, 45, 50, 60, 70, 75 deg. Conversely, the other 27 cases unsuccessfully converge to the target angles, therefore, the gimbals do not satisfy repeatability. This is because the CMG system encounters elliptic singularities, as explained in Sec. II.B. In the 10 successful cases, 5 cases (d = 45, 50, 60, 70, 75 deg) present better performances because m is larger and t_{m0} and s_{m0} are smaller than those in Case 1 (Figure 1). Similarly, in Case 3 (Figure 3), the gimbals converge to the final target gimbal angles $\boldsymbol{\delta}_{Fb}$ when d = 105, 110, 120, 135, 150 deg, and these performances are better than those of Case 1. The 24 other cases unsuccessfully converge for the same reason as Case 2. Therefore, a total of 10 sets, shown by gray hatches in Figures 2 and 3, are identified as desirable final gimbal angles.

C. Typical Simulation Results

1. Simulation Results in case of d = 0 deg

Some typical results of the many simulation cases summarized in Figure 2 are illustrated as examples. Figure 4 shows the case of $\boldsymbol{\delta}_F = [0\ 0\ 0\ 0]^T$ deg in accordance with d = 0 deg (Case 2a), which is same as the initial gimbal angles $\boldsymbol{\delta}_0$ from the first maneuver. As can be seen in Figure 4a, the gimbal angles at the end of each maneuver converge to the final angles $\boldsymbol{\delta}_F$. When the CMG system encounters some singularities, the total gimbal rate $\dot{\boldsymbol{\delta}}_V$ becomes large and is limited by $\dot{\delta}_i^{lmt} = \pm 1.0 \text{rad/s}$ (Figure 4b). Figure 4c shows that the quadratic form η_{SV} simultaneously rises with decreasing CMG gain, as described in Sec. II.B. Simultaneously, as the quadratic form increases, the null motion term L_{SV} of the Lyapunov function decreases, as shown in Figure 4d. The offsets of the total Lyapunov function L_V come from the gimbal rate limit, which occurs for the even-numbered maneuvers. When the CMG system encounters singularities, the steering law based on a singularity-robust inverse induces torque errors, which results in attitude errors. Despite these instantaneous attitude errors during slewings, the errors converge to zero due to high-bandwidth feedback control. This indicates that the attitude control by torqued motion does not interfere with gimbal angle control by null motion and vice versa.

2. Simulation Results in case of d = 60 deg

Figure 5 shows the case of $\boldsymbol{\delta}_F = [60\ -60\ 60\ -60]^T$ deg in accordance with d = 60 deg (Case 2b). As addressed above, the steering law performs optimally when d = 60 deg, with a mean value of the CMG gain $m \approx 1.2$ (Figure 2a), a number of times $s_{m0} = 1$ (Figure 2b), and a total duration $t_{m0} < 1$ s (Figure 2c). As can be seen in Figure 5a, the gimbal angles at the end of each maneuver converge to the final angles $\boldsymbol{\delta}_F$, with a small gimbal rate (Figure 5b) compared with that of Figure 4b. Figure 5c shows that the null motion keeps the gimbals away from the singularity during ten maneuvers and traverses only one singularity, which is encountered approximately 10 s after the beginning of the first slewing. Therefore, the steering law can reduce the occurrence and total duration of singularities if the gimbals are steered to desirable final angles, as specified in Figures 2 and 3. The other nine cases, shown as gray hatches in Figures 2 and 3, present similar results. In the literature [3], the gimbal angles $[45\ -45\ 45\ -45]^T$ deg in accordance with d = 45 deg of our simulation cases were specified as “preferred sets of initial gimbal angles” to avoid singularity. However, it was assumed that the initial gimbal reorientation is performed prior to slewings using solo null motion. On the contrary, in our steering strategy, the gimbal angle control by null motion is performed during slewings with the torqued motion. Our combined steering law with specified desirable final angles

is more effective at reducing total maneuver time than that of [3], better at keeping the gimbals away from singularities than that of [14], and has a simpler implementation for conventional CMG than that of [5]. This is the main contribution of our Note.

D. Performance of the Modified Steering Law

1. Simulation Results in case of d = −60 deg

Figure 6 shows the case of $\boldsymbol{\delta}_F = [-60\ 60\ -60\ 60]^T$ deg in accordance with d = −60 deg (Case 2c). Although this case presents better performances than Case 1, as shown in Figure 2, the gimbals do not converge to the final angles $\boldsymbol{\delta}_F$ at the end of each maneuver, as shown in Figure 6a. In particular, the gimbal angles at the end of even-numbered maneuvers have large offsets with respect to their target angles, while their gimbal rate is within the limit $\pm 1.0 \text{rad/s}$ (Figure 6b). Figure 6c reveals that the magnitude of the quadratic form η_{SV} remains almost at zero after 140 s in the second maneuver, where the gimbal angles approach undesirable final angles. Consequently, as shown in Figure 6d, the null motion term L_{SV} does not decline to cancel out the torqued motion term L_{TV}, and the total Lyapunov function L_V does not converge to zero at the end of the second maneuver. The behavior of subsequent even-numbered maneuvers is explained, as well as that of the second maneuver. It is evident that the CMG system fails to yield effective null motion, as it encounters elliptic singularities in even-numbered maneuvers.

2. Simulation Results in case of d = −60 deg with modified steering law

Figure 7 displays Case 2d, which applies the modified steering law (Eq. (20)) under the same conditions as Case 2c. The time-varying scaling factor λ_W (Eq. (23)) is applied when the CMG system is producing deceleration torque in even-numbered maneuvers. The diagonal elements of Eq. (22) are selected as $\mathbf{E}_W = \text{diag}[1 \quad 0.05 \quad 0.05 \quad 1]$. Figure 7a shows that the modified steering law can steer the gimbals to their final angles $\boldsymbol{\delta}_F = [-60\ 60\ -60\ 60]^T$ deg at the end of even-numbered maneuvers. Although the total gimbal rate reaches the limit $\pm 1.0 \text{rad/s}$ at 140 s (Figure 7b), this does not affect the convergence of the gimbal angles. Figure 7c shows that the magnitude of the quadratic form η_{SVW} is changed at 140 s and immediately increased at approximately 150 s. While the CMG system encounters a new singularity ($m \approx 0$) at approximately 150 s, the null motion term L_{SVW}

declines sufficiently to cancel out the torqued motion term L_{TVW}, as shown in Figure 7d. We can calculate the unit null motions $\bar{\dot{\boldsymbol{\delta}}}_{NV}$ for Case 2c and $\bar{\dot{\boldsymbol{\delta}}}_{NVW}$ for Case 2d at 150 s, as follows:

$$\bar{\dot{\boldsymbol{\delta}}}_{NV} = \mathbf{S}_V \mathbf{e} = \begin{bmatrix} 0.259 & -0.205 & -0.007 & -0.386 \\ -0.205 & 0.164 & 0.007 & 0.307 \\ -0.007 & 0.007 & 0.001 & 0.012 \\ -0.386 & 0.307 & 0.012 & 0.578 \end{bmatrix} \begin{bmatrix} -0.218 \\ -1.055 \\ 1.534 \\ 0.307 \end{bmatrix} = \begin{bmatrix} 0.031 \\ -0.023 \\ -0.001 \\ -0.044 \end{bmatrix} \tag{24}$$

$$\bar{\dot{\boldsymbol{\delta}}}_{NVW} = \mathbf{S}_{VW} \mathbf{e} = \begin{bmatrix} 0.541 & 0.043 & 0.482 & -0.406 \\ 0.002 & 0.900 & 0.081 & 0.024 \\ 0.024 & 0.081 & 0.904 & 0.003 \\ -0.406 & 0.476 & 0.052 & 0.539 \end{bmatrix} \begin{bmatrix} -0.464 \\ -0.877 \\ 1.166 \\ 0.458 \end{bmatrix} = \begin{bmatrix} 0.087 \\ -0.685 \\ 0.973 \\ 0.078 \end{bmatrix} \tag{25}$$

As described in Sec. III.C, the steering law (Eq. (1)) fails to generate the effective unit null motion $\bar{\dot{\boldsymbol{\delta}}}_{NV}$, which is almost zero, as illustrated in Eq. (24). Conversely, the weighting matrix $\mathbf{W}$ in the modified steering law (Eq. (20)) yields change for the matrix $\mathbf{S}_{VW}$ and boosts the substantial unit null motion $\bar{\dot{\boldsymbol{\delta}}}_{NVW}$, as illustrated in Eq. (25). The gimbal angle convergence in subsequent even-numbered maneuvers as well as in the second maneuver is improved. It is also successfully verified that the modified steering law can maintain repeatability and can effectively steer gimbals to final target gimbal angles, which is another significant contribution from this Note.

Table 1 Simulation parameters

Parameter	Value
Initial gimbal angles $\boldsymbol{\delta}_0$	$[0\ 0\ 0\ 0]^T$ deg
Final target gimbal angles $\boldsymbol{\delta}_F$	Figure 2 for Case 2 Figure 3 for Case 3
Rotor angular momentum h_R	30 Nms
CMG skew angle β	54.74 deg
Null motion gain K_N	1 s^{-1}
Gimbal rate limit $\dot{\delta}_i^{lmt}$	$\pm$ 1.0 rad/s
Parameters for weighting matrix $\mathbf{V}$	$\lambda_{V0} = 0.1$, $\mu_V = 10$, $\varepsilon_{V0} = 0.01$, $\omega_V = 0.5\pi$, $\phi_1 = 0$, $\phi_2 = \pi/2$, $\phi_3 = \pi$
Parameters for weighting matrix $\mathbf{W}$ (only for Case 2d)	$\lambda_{W0} = 1.0$, $\mu_W = 1.0$, $\varepsilon_{W1} = \varepsilon_{W4} = 1.0$, $\varepsilon_{W2} = \varepsilon_{W3} = 0.05$
Inertia of spacecraft $\mathbf{I}$	diag [3000 3000 2000] kgm^2
The bandwidth f_S of PD feedback control	0.5 Hz
The damping ratio ζ_S of PD feedback control	$1/\sqrt{2}$

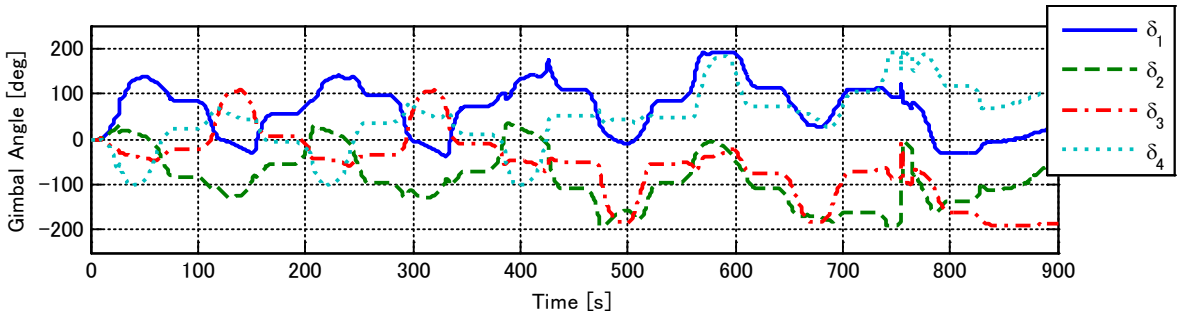

a) Gimbal angle δ

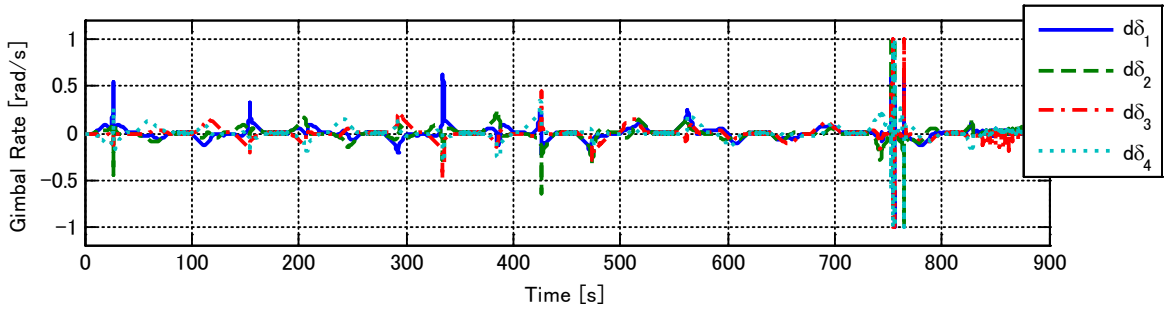

b) Gimbal rate $\dot{\delta}_{TV}$ (torqued motion only)

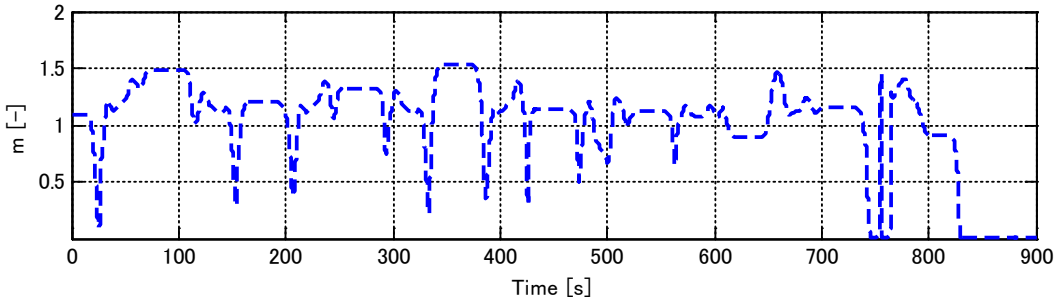

c) CMG gain m

Fig. 1 Simulation results for Case 1: without gimbal angle control ($K_N = 0$)

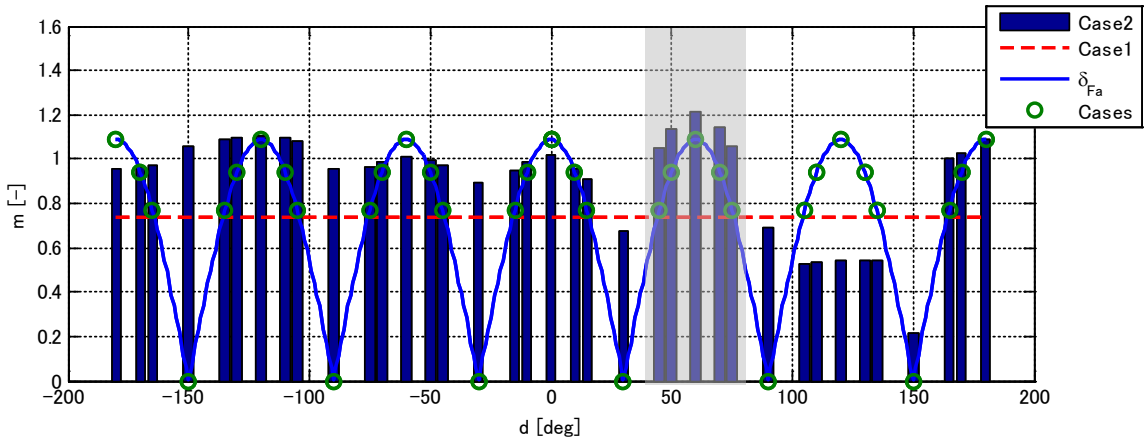

a) Mean value of CMG gain m

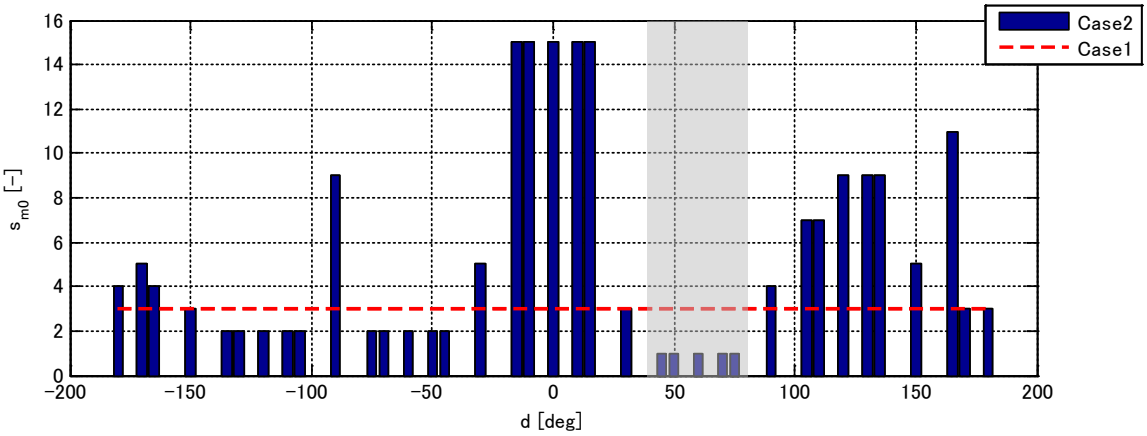

b) Occurrence of singularities s_{m0}

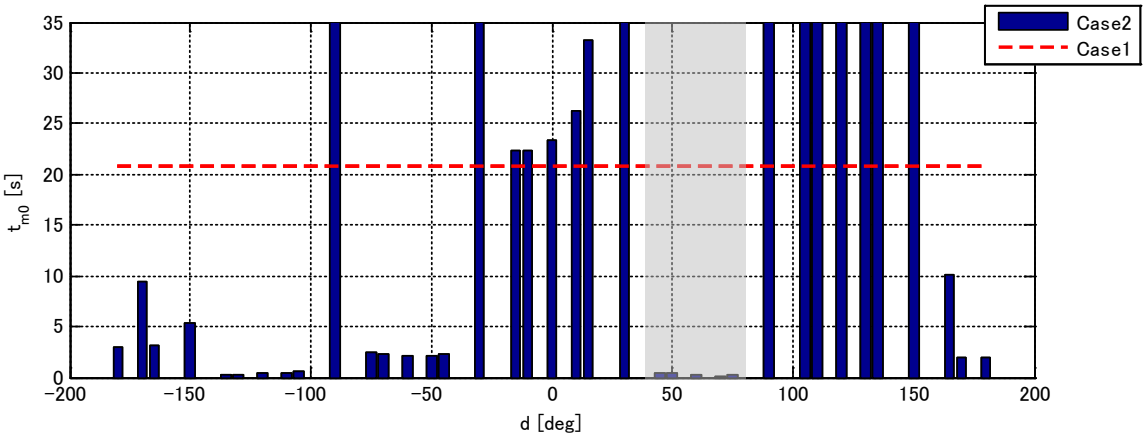

c) Total duration of singularities t_{m0}

Fig. 2 Simulation results for Case 2: δ_{Fa} = [d −d d −d]^{T}deg

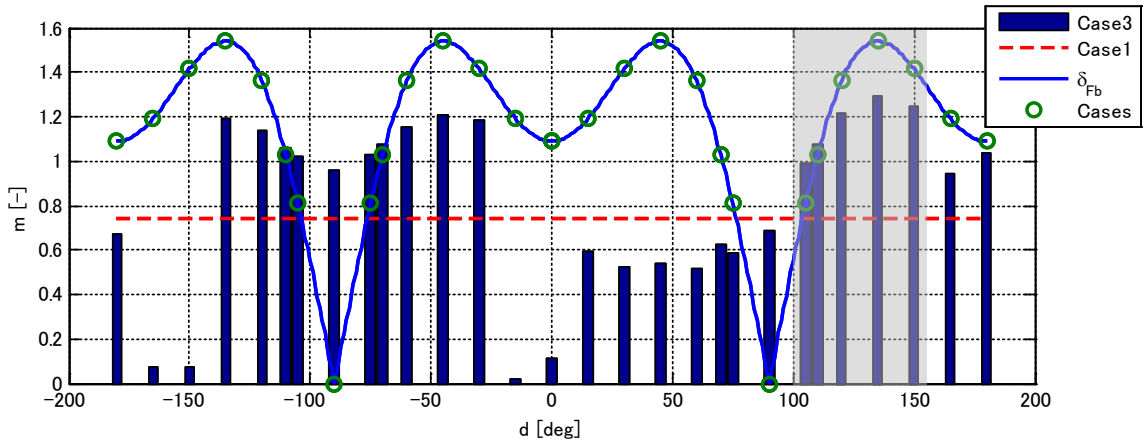

a) Mean value of CMG gain m

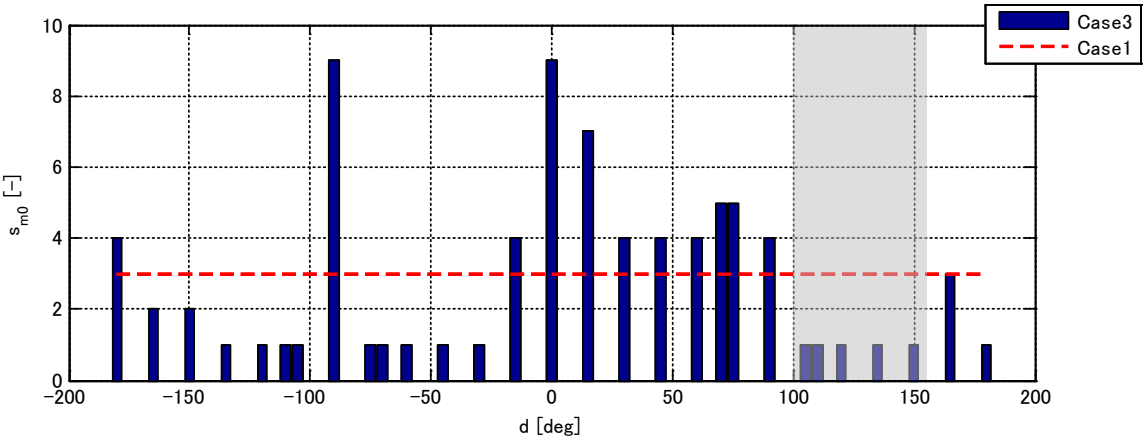

b) Occurrence of singularities s_{m0}

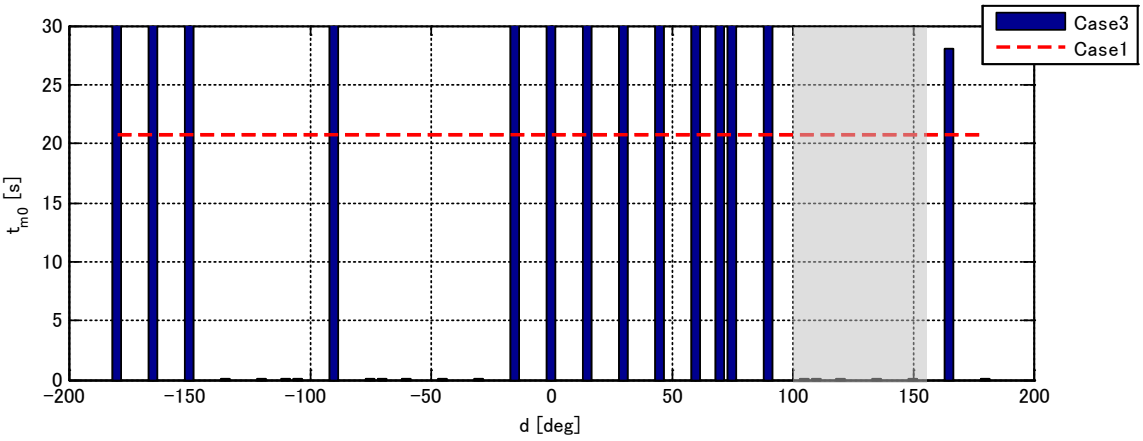

c) Total duration of singularities t_{m0}

Fig. 3 Simulation results for Case 3: $\delta_{Fb} = [d\ d\ -\pi\ \ d\ d\ -\pi\ ]^T deg$

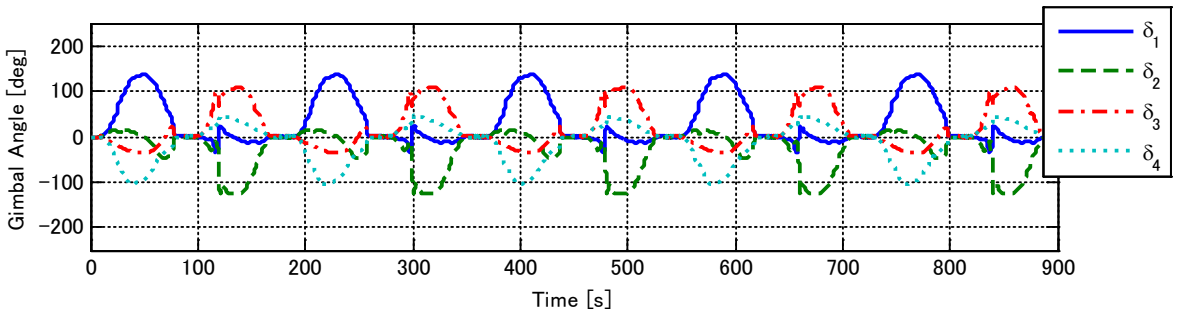

a) Gimbal angle δ

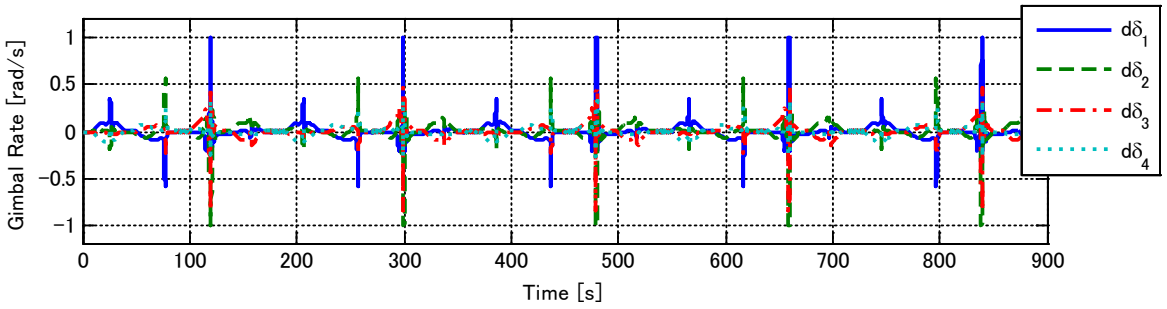

b) Total gimbal rate $\dot{\delta}_V$

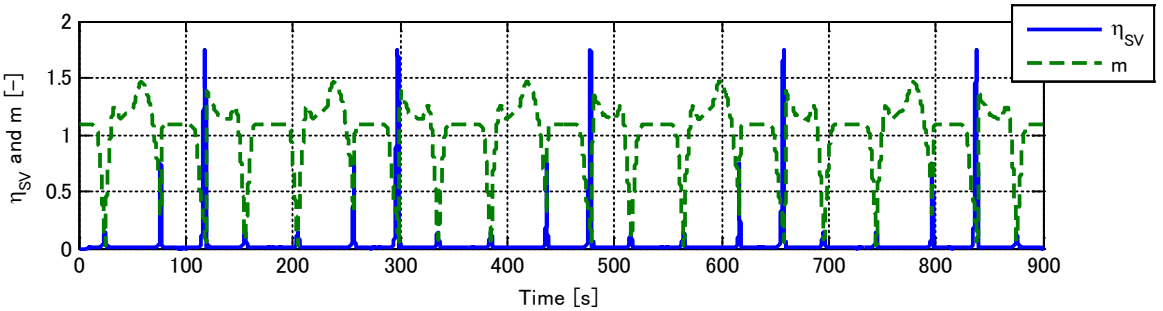

c) Quadratic form η_{SV} and CMG gain m

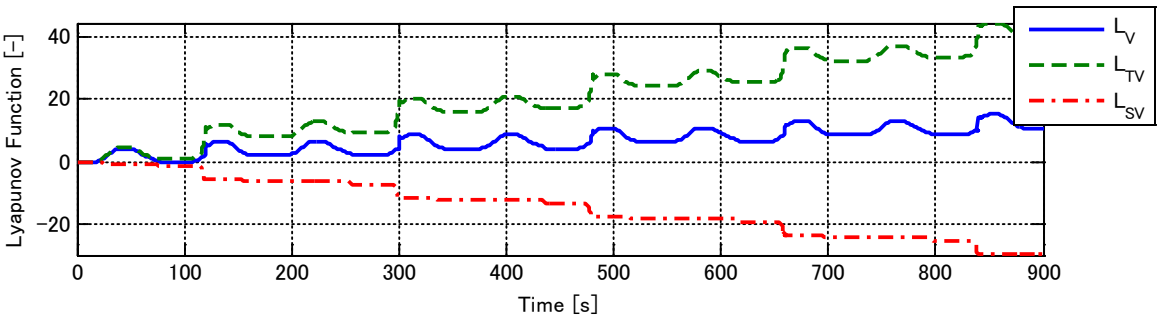

d) Lyapunov functions L_V, L_{TV} and L_{SV}

Fig. 4 Simulation results for Case 2a: $\delta_F = [0\ 0\ 0\ 0]^T$deg

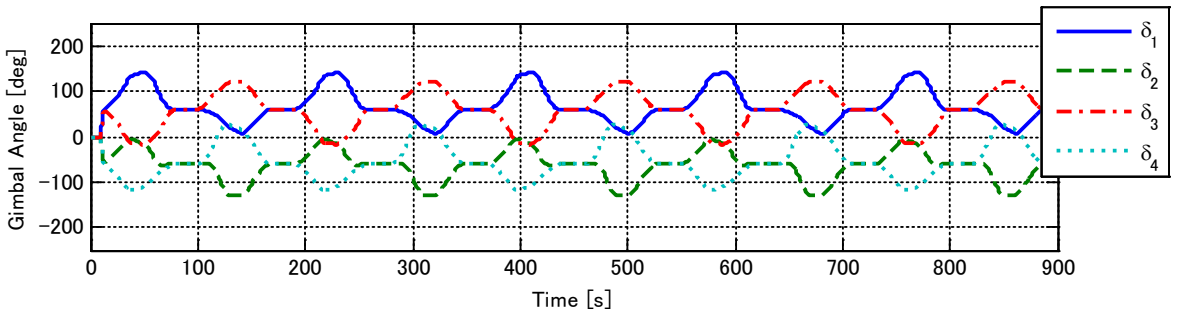

a) Gimbal angle δ

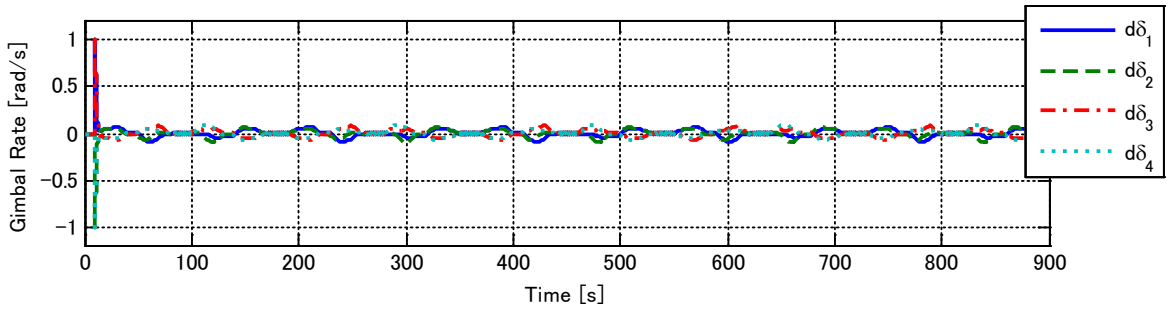

b) Total gimbal rate $\dot{\delta}_V$

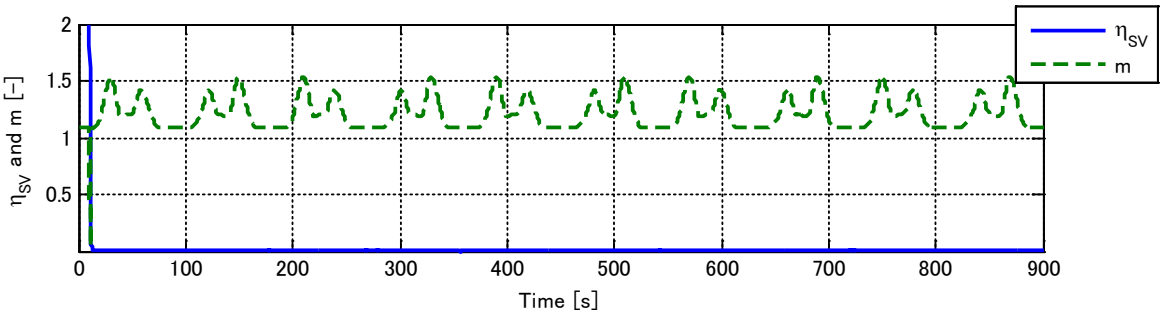

c) Quadratic form η_{SV} and CMG gain m

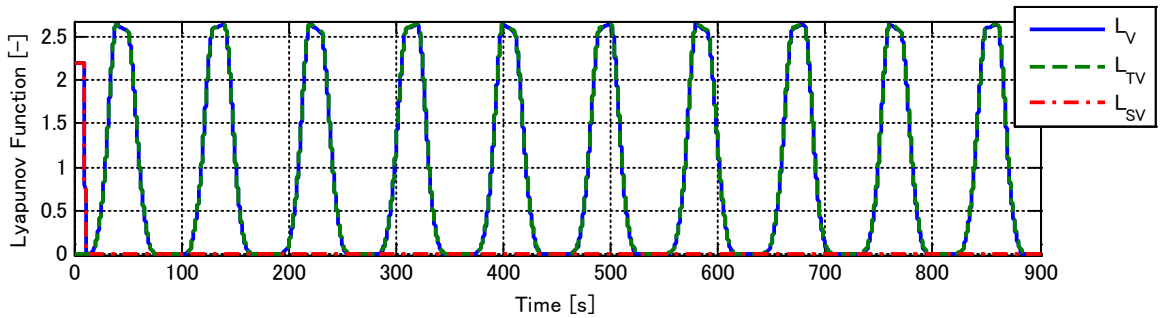

d) Lyapunov functions L_V, L_{TV} and L_{SV}

Fig. 5 Simulation results for Case 2b: δ_F = [60 −60 60 −60]^{T}deg

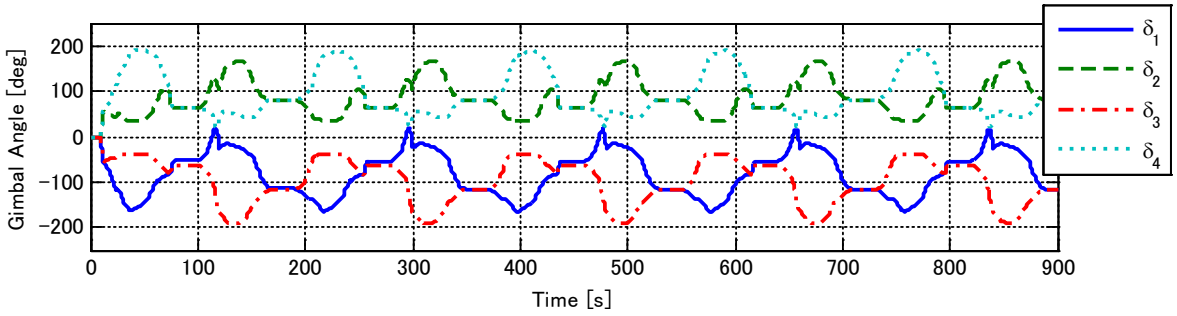

a) Gimbal angle δ

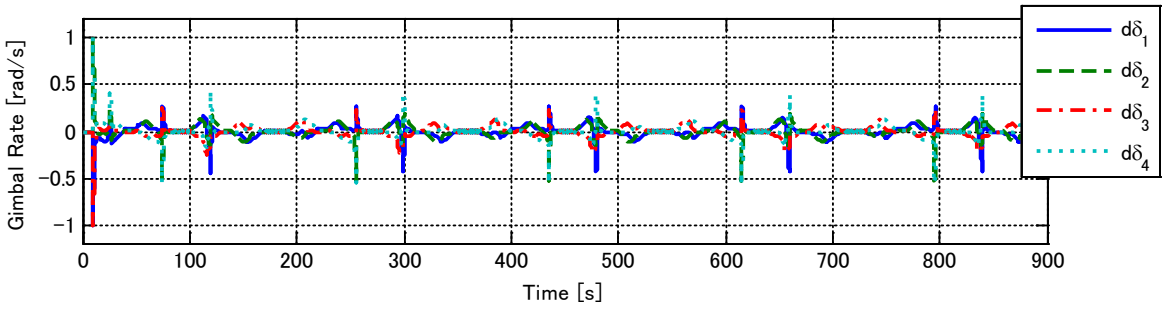

b) Total gimbal rate $\dot{\delta}_V$

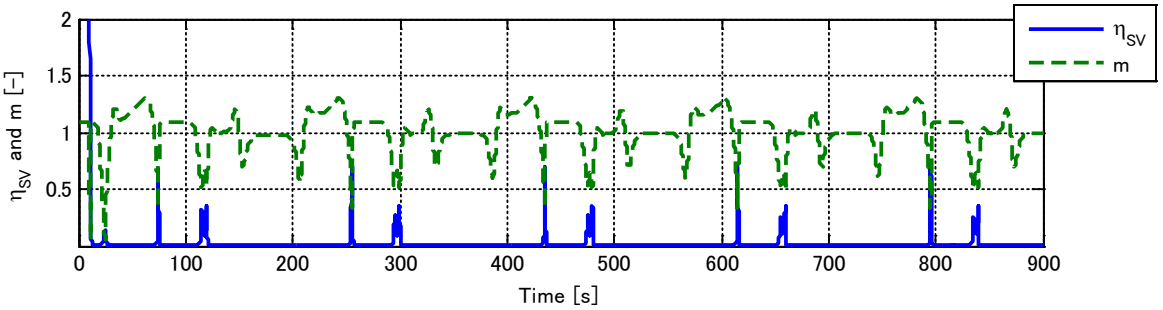

c) Quadratic form η_{SV} and CMG gain

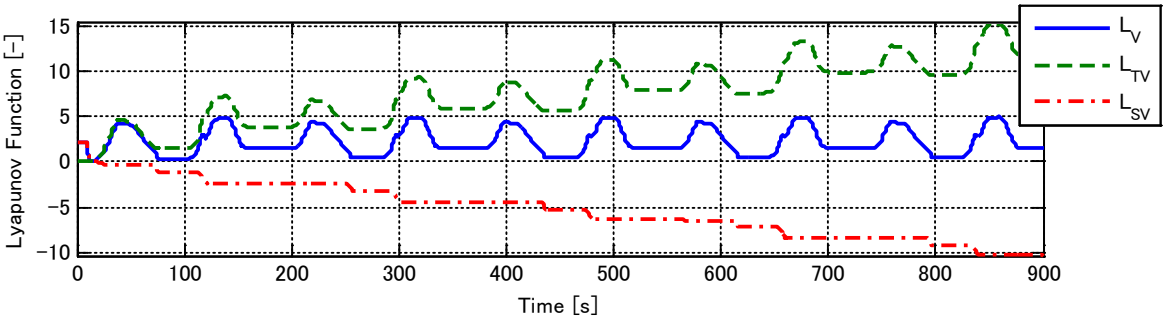

d) Lyapunov functions L_V, L_{TV}, and L_{SV}

Fig. 6 Simulation results for Case 2c: $\delta_F = [-60\ 60\ -60\ 60]^T$ deg

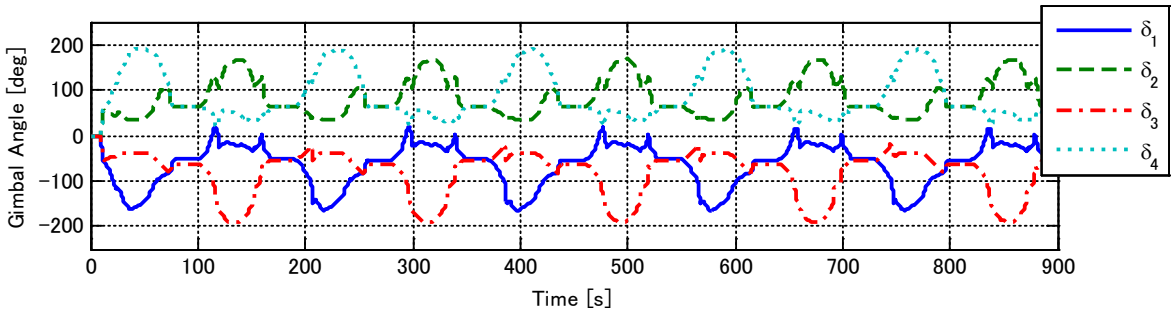

a) Gimbal angle δ

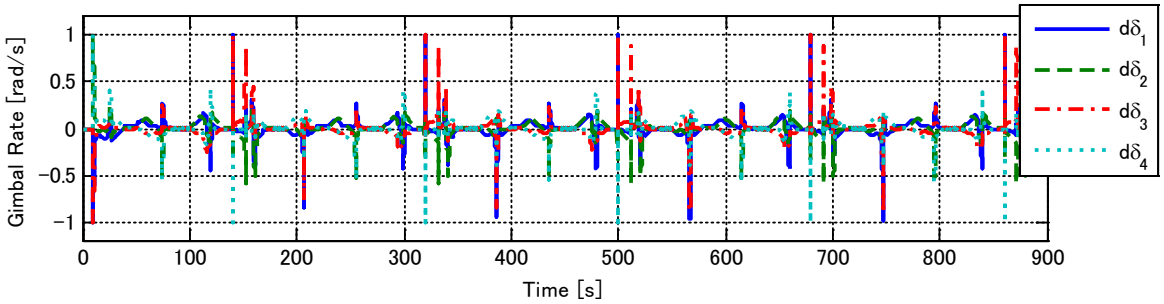

b) Total gimbal rate $\dot{\delta}_V$

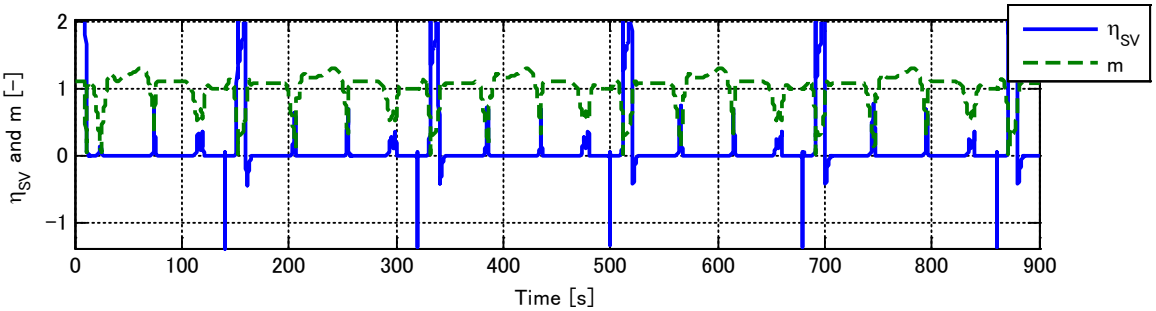

c) Quadratic form η_{SVW} and CMG gain m

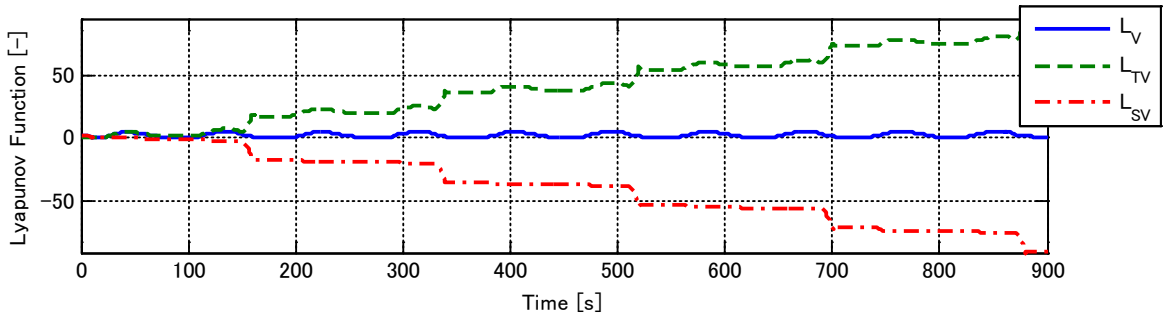

d) Lyapunov functions L_{VW}, L_{TVW}, and L_{SVW}

Fig. 7 Simulation results for Case 2d: δ_F = [−60 60 −60 60]^T deg

V. Conclusions

This Note presented a steering law that not only provides the required attitude control torque but also controls the gimbals to their final target gimbal angles, eliminating the need for gimbal reorientation in agile, large-angle and rest-to-rest multitarget maneuvers. The stability of the gimbal angle control is analyzed using a Lyapunov function, and it is shown that convergence to the final angles declines when the quadratic form becomes too small. To improve convergence, the steering law is modified by including a weighting matrix, which depends on the prescribed feedforward torque profile. On the basis of numerical simulations and considering some performance metrics, the following advances are demonstrated. First, a simply implemented steering law with desirable final gimbal angles is identified as an effective means to reduce total maneuver time and to steer the gimbals away from singularities. Second, a modified steering law effectively converges gimbals to their final angles and resolves the issue of repeatability. Consequently, a spacecraft could continuously perform agile multitarget maneuvers.

References

[1] Kurokawa, H., "Survey of Theory and Steering Laws of Single-Gimbal Control Moment Gyros," *Journal of Guidance, Control and Dynamics*, Vol. 30, No. 5, 2007, pp. 1331-1340.
doi:10.2514/1.27316

[2] Jones, L. L., Zeledon, R. A. and Peck. M. A., "Generalized Framework for Linearly Constrained Control Moment Gyro Steering," *Journal of Guidance, Control and Dynamics*, Vol. 35, No. 4, 2012, pp. 1094-1103.
doi:10.2514/1.56207

[3] Vadali, S. R., Oh, H. S. and Walker S. R., "Preferred Gimbal Angles for Single Gimbal Control Moment Gyros," *Journal of Guidance, Control and Dynamics*, Vol. 13, No. 6, 1990, pp. 1090-1095.
doi:10.2514/3.20583

[4] Nanamori, Y. and Takahashi, M., "Steering Law of Control Moment Gyros using Optimization of Initial Gimbal Angles for Satellite Attitude Control," *Journal of System Design and Dynamics*, Vol. 5, No. 1, 2011, pp. 30-41.
doi:10.1299/jsdd.5.30

[5] Schaub, H. and Junkins, J.L., "Singularity Avoidance Using Null Motion and Variable-Speed Control Moment Gyros," *Journal of Guidance, Control, and Dynamics*, Vol. 23, No.1, 2000, pp. 11-16.
doi:10.2514/2.4514

[6] MacMahon, J. and Schaub, H., "Simplified Singularity Avoidance Using Variable-Speed Control Moment Gyroscope Null Motion," *Journal of Guidance, Control, and Dynamics*, Vol. 32, No. 6, 2009, pp. 1938-1943.
doi:10.2514/1.45433

[7] Leeghim, H., Bang, H., and Park, J.-O., "Singularity avoidance of control moment gyros by one-step ahead singularity index," *Acta Astronautica*, Vol. 64, No. 9-10, 2009, pp. 935-945.
doi:10.1016/j.actaastro.2008.11.004

[8] Yoon, H. and Tsiotras, P., "Spacecraft Adaptive Attitude and Power Tracking with Variable Speed Control Moment Gyroscopes," *Journal of Guidance, Control, and Dynamics*, Vol. 25, No. 6, 2002, pp. 1081-1090.
doi:10.2514/2.4987

[9] Vadali, S. R. and Krishnan, S., "Suboptimal Command Generation for Control Moment Gyroscopes and Feedback Control of Spacecraft," *Journal of Guidance, Control and Dynamics*, Vol. 18, No. 6, 1995, pp. 1350-1354.
doi:10.2514/3.21552

[10] Avanzini, G. and Matteis, G., "A Local Optimization Technique for Attitude Motion Tracking Using Control Moment Gyroscopes," *The Journal of the Astronautical Sciences*, Vol. 50, No. 2, 2002, pp. 213-229.

[11] Ohmura, T., "Convergence and Optimality of Control Law for Periodic Maneuvering Satellites with CMGs," 18th IFAC Symposium on Automatic Control in Aerospace, 2010, pp. 548-553.
doi:10.3182/20100906-5-JP-2022.00093

[12] Bedrossian, N. S., Paradiso, J., Bergmann, E. V. and Rowell, D., "Steering Law Design for Redundant Single-Gimbal Control Moment Gyroscopes," *Journal of Guidance, Control and Dynamics*, Vol. 13, No. 6, 1990, pp. 1083-1089.
doi:10.2514/3.20582

[13] Ford, K. A. and Hall, C. D., "Singular Direction Avoidance Steering for Control-Moment Gyros," *Journal of Guidance, Control and Dynamics*, Vol. 23, No. 4, 2000, pp. 648-656.
doi:10.2514/2.4610

[14] Wie, B., Bailey, D. and Heiberg, C., "Singularity Robust Steering Logic for Redundant Single-Gimbal Control-Moment Gyros," *Journal of Guidance, Control and Dynamics*, Vol. 24, No. 5, 2001, pp. 865-872.
doi:10.2514/2.4799

[15] Wie, B., "New Singularity Escape/Avoidance Steering Logic for Control-Moment Gyro Systems," AIAA Guidance, Navigation and Control Conference, AIAA 2003-5659, Austin, TX, 2003.
doi:10.2514/6.2003-5659

[16] Wie, B., Bailey, D. and Heiberg, C., "Rapid Multitarget Acquisition and Pointing Control of Agile Spacecraft," *Journal of Guidance, Control and Dynamics*, Vol. 25, No. 1, 2002, pp. 96-104.

doi:10.2514/2.4854

[17] Giffen, A., Palmer, P.L. and Roberts, R.M., "Exact CMG Steering Laws which Reset Gimbal Angles," Surrey Space Centre Research, URL: http://surreyspacecentre.wordpress.com/2012/11/27/exact-cmg-steering-laws-which-reset-gimbal-angles-2/ [cited 2 November, 2012].

[18] Asghar, S., Palmer, P. L. and Roberts, M., "Exact steering law for pyramid-type four control moment gyro systems," AIAA/AAS Astrodynamics Specialist Conference and Exhibit, AIAA 2006-6652, Keystone, CO, 2006.
doi:10.2514/6.2006-6652

[19] Kim, J. J. and Agrawal, B. N., "Rest-to-Rest Slew Maneuver of Three-Axis Rotational Flexible Spacecraft," Proceedings of the 17th World Congress The International Federation of Automatic Control, Seoul, Korea, 2008, pp. 12054-12060.
doi:10.3182/20080706-5-KR-1001.02040

[20] Richie, D. J., Lappas, V. J. and Palmer, P. L., "Sizing/Optimization of Small Satellite Energy Storage and Attitude Control System," *Journal of Spacecraft and Rockets*, Vol. 44, No.4, 2007, pp. 940-952.
doi:10.2514/1.25134

[21] Strang, G., Linear Algebra and Its Applications, 2nd ed., Academic Press, New York, 1980.

[22] Schaub, H. and Junkins, J. L., Analytical Mechanics of Space Systems, AIAA Education series, AIAA, Reston, VA, 2003, p. 309.

[23] Bedrossian, N. S., Paradiso, J., Bergmann, E. V. and Rowell, D., "Redundant Single Gimbal Control Moment Gyroscope Singularity Analysis," *Journal of Guidance, Control and Dynamics*, Vol. 13, No. 6, 1990, pp. 1096-1101.
doi:10.2514/3.20584

[24] Wie, B., "Singularity Analysis and Visualization for Single-Gimbal Control Moment Gyro Systems," *Journal of Guidance, Control and Dynamics*, Vol. 27, No. 2, 2004, pp. 271-282.
doi:10.2514/1.9167

[25] Leve, F. A. and G. Fitz-Coy. Norman., "Hybrid Steering Logic for Single-Gimbal Control Moment Gyroscopes," *Journal of Guidance, Control and Dynamics*, Vol. 33, No. 4, 2010, pp. 1202-1212.
doi:10.2514/1.46853